Synergistic Band Engineering and Ferroelectric Polarization in Sn/S Co-doped $BaTiO_3$ for Integrated Photovoltaic-Energy Storage

*Mei Wu[a], Zheng Kang[a], Dan Lin[a], Yunkai Wu[*a],Xu Wang[**b]*

a: College of Big Data and Information Engineering, Guizhou University, Guiyang, 550025, Guizhou, China

b: Key Laboratory of Advanced Manufacturing Technology, Ministry of Education, Guiyang, 550025, Guizhou, China

*Corresponding author. E-mail: ykwu@gzu.edu.cn

**Corresponding author. E-mail: xuwang@gzu.edu.cn

Note S1: The tolerance factor was proposed by Goldschmidt to evaluate the structural stability of ABO_3-type perovskites. Its calculation formula is as follows:

$$t = \frac{r_A + r_O}{\sqrt{2}(r_B + r_O)}$$

where r_A, r_B, and r_O represent the ionic radii of the A-site cation, B-site cation, and O-site anion, respectively. It is generally considered that a stable perovskite structure can form when $0.8 \leq t \leq 1.1$. The octahedral factor is used to assess the stability of the $[BX_6]$ octahedra in ABO_3-type perovskite structures, with its calculation formula given by:

$$\mu = \frac{r_B}{r_O}$$

It is typically believed that the $[BX_6]$ octahedra can stably exist when $0.414 \leq \mu \leq 0.732$.

Table S1. Optimized structural and electronic property parameters of BTO with different sizes.

Size	a(Å)	b(Å)	c(Å)	c/a	α	β	γ	V(Å^3)	Space Group	E_g
1x1x1	3.968	3.968	4.068	1.025	90°	90°	90°	64.050	P4mm	1.766
2x2x2	3.968	3.968	4.067	1.025	90°	90°	90°	64.031	P4mm	1.766
3x3x3	3.967	3.967	4.069	1.026	90°	90°	90°	64.041	P4mm	1.766

Table S2. The Formation energy of BTSOS

Material	E_{BTSOS}	E_{BTO}	μ_{Sn}	μ_S	μ_{Ti}	μ_O	E_f
BTSOS	-322.401	-320.307	-4.226	-3.330	-8.275	-3.381	-6.194

Note S2: For a tetragonal crystal system, according to Born's stability criteria, its elastic constants(C_{ij}) must satisfy the following conditions to ensure mechanical stability[1]:

$$C_{11} > 0, C_{33} > 0, C_{44} > 0, C_{66} > 0$$

$$C_{11} - C_{12} > 0$$

$$C_{11} + C_{33} - 2C_{13} > 0$$

$$2C_{13}^2 < C_{33}(C_{11} + C_{12})$$

$$2C_{11} + C_{33} + 2C_{12} + 4C_{13} > 0$$

Note S3: Based on the elastic constants, the Voigt-Reuss-Hill method was employed to calculate key mechanical properties of the materials, including bulk modulus (B), shear modulus (G), Young's modulus (E), and Poisson's ratio (v). This method integrates the widely used Voigt (V) approximation and Reuss (R) approximation; the aforementioned mechanical parameters can be accurately derived by combining the calculation results of the two approximations, providing reliable and effective support for in-depth analysis of the materials' mechanical properties.

$$B_V = \frac{1}{9}[(C_{11} + C_{22} + C_{33}) + 2(C_{12} + C_{23} + C_{31})]$$

$$G_V = \frac{1}{15}[(C_{11} + C_{22} + C_{33}) - (C_{12} + C_{23} + C_{31}) + 3(C_{44} + C_{55} + C_{66})]$$

$$B_R = [(S_{11} + S_{22} + S_{33}) + 2(S_{12} + S_{23} + S_{31}]^{-1}$$

$$G_R = 15[4(S_{11} + S_{22} + S_{33}) - (S_{12} + S_{13} + S_{23}) + 3(S_{44} + S_{55} + S_{66})]^{-1}$$

The Voigt and Reuss equations can respectively provide the upper and lower bounds of the estimated elastic modulus of materials.

$$B = \frac{1}{2}(B_V + B_R)$$

$$G = \frac{1}{2}(G_V + G_R)$$

$$E = \frac{9BG}{3B + G}$$

$$\nu = \frac{3B - 2G}{2(3B + G)}$$

The bulk modulus measures a material's resistance to hydrostatic pressure; the higher the bulk modulus, the more difficult it is to compress the material. The shear modulus describes a material's resistance to shear stress; the higher the shear modulus, the greater the material's rigidity under shear forces. Young's modulus measures a material's stiffness under uniaxial tension or compression; the higher the Young's modulus, the greater the material's rigidity during tension or compression.

Table S3. The Bulk Modulus (GPa), Shear Modulus (GPa), Young's Modulus (GPa), Poisson's Ratio (ν), and B/G Ratio of BTO and BTSOS

Material	B	G	E	ν	B/G	Ref.
BTO	135.130	82.434	205.511	0.247	1.639	This work
BTO	138	94	230	0.28	1.47	1
BTO	132	68	174	0.27	1.94	2
BTSOS	138.474	80.430	202.151	0.257	1.722	This work

Table S4. The Bader Charge Analysis of BTO and BTSOS

Material	Atom	Valence Charge(e)	Bader Charge(e)	Charge Transfer(e)
BTO	Ba	+10	+8.455	+1.545
	Ti	+12	+9.850	+2.150
	O	+6	+7.232	-1.232
BTSOS	Ba	+10	+8.959	+1.041
	Ti	+12	+9.899	+2.101
	Sn	+14	+11.629	+2.371
	O	+6	+7.074	-1.074
	S	+6	+6.695	-0.695

Note S4: The real and imaginary parts of the complex dielectric constant($\varepsilon(\omega)$) can be expressed using the following formulas:

$$\varepsilon_2(\omega) = \frac{2\pi e^2}{\Omega\varepsilon_0}\sum_{k,v,c}\left\langle\Psi_k^c\middle|\hat{u}.r\middle|\Psi_k^v\right\rangle^2\delta\left(E_k^c - E_k^v - \hbar\omega\right)$$

$$\varepsilon_1(\omega) = 1 + \frac{2}{\pi}P\int_0^{\infty}\frac{\varepsilon_2(\omega')\omega'}{\omega'^2 - \omega^2}d\omega'$$

where e represents the charge carried by an electron, ε_0 denotes the vacuum dielectric constant, Ω refers to the volume, and $\hbar\omega$ is the energy of the incident phonon. The subscripts c and v correspond to the conduction band and valence band, respectively. u is the vector defining the polarization direction of the incident electric field, r represents the momentum operator, Ψ_k^c and Ψ_k^v are the wave functions of the conduction band and valence band at the k-point, respectively, and P stands for the principal value of the integral.

Note S5: The light absorption coefficient α(ω) can be calculated using the following formula[3, 4]:

$$\alpha(\omega) = \frac{\sqrt{2}\omega}{c}\left[\sqrt{\varepsilon_1(\omega)^2 + \varepsilon_2(\omega)^2} - \varepsilon_1(\omega)\right]^{\frac{1}{2}}$$

Note S6: The short-circuit current density (J_{sc}) is used to characterize the maximum current output capability of a photovoltaic device under short-circuit conditions. Its magnitude directly depends on the generation and collection efficiency of photogenerated carriers, and can be expressed by the following formula[5-7]:

$$J_{sc} = e\int_0^{\infty} A(E) I_{sun}(E) dE$$

Where $I_{sun}(E)$ describes the solar photon flux under the condition of a specific energy E. In this study, the AM 1.5 standard solar spectrum is selected to determine its value[8]. And e represents the elementary charge. For an absorber layer with a reflective back surface and a thickness of L, its light absorption rate A(E) needs to account for the secondary reflection effect of photons inside the absorber layer. Therefore, it can be calculated using the formula $A(E)=1-e^{-2\alpha(E)L}$[9].

The reverse saturation current density (J_0) reflects the total recombination rate of electron-hole pairs in semiconductor materials under dark, equilibrium conditions, which serves as a core parameter characterizing the dark current loss in photovoltaic devices.

Its essence is composed of non-radiative (J_0^{nr}) and radiative (J_0^{r}) recombination current densities. $I_{bb}(E,T)$ represents the blackbody radiation flux corresponding to photons with energy E at temperature T. f_r represents the proportion of radiative recombination current. When modeled using the Boltzmann factor, it requires

integration with the material's bandgap characteristics (including the fundamental bandgap(E_g) and the direct-allowed bandgap (E_g^{da})). The specific formula is as follows[10, 11]:

$$J_0 = J_0^{nr} + J_0^r = \frac{J_0^r}{f_r}$$

$$J_0^r = e\int_0^{\infty} A(E) I_{bb}(E,T) dE$$

$$f_r = e^{\left(\frac{E_g^{da} - E_g}{KT}\right)}$$

where Krepresents the Boltzmann constant, and T denotes the temperature. For the direct bandgap semiconductor BTSOS, electron-hole recombination is predominantly radiative, with negligible contributions from non-radiative processes. Under such conditions, f_r=1，$J_0 \approx J_0^r$. This behavior is closely tied to the electronic transition mechanism in direct bandgap semiconductors, where electrons transition from the conduction band to the valence band without phonon assistance, releasing energy in the form of photons. This significantly reduces non-radiative losses, constituting one of the core advantages of BTSOS for photovoltaic applications.

The photoelectric conversion efficiency (PCE) characterizes the ability of a photovoltaic device to convert incident light energy into electrical energy, and can be expressed by the following formula:

$$\mathrm{PCE} = \frac{\mathrm{P_{max}}}{\mathrm{P_{in}}}$$

where $\mathrm{P_{in}}$ denotes the total incident power density of the solar spectrum, with its value specified as 1000.37 W/m² under the standard AM 1.5G solar spectrum commonly adopted in photovoltaic research.$\mathrm{P_{max}}$ represents the maximum power density (W/m²) of the device, whose numerical value must be derived from the current density-voltage (J-V) characteristics of the solar cell. Specifically, it corresponds to the maximum power point(MPP) on the J-V characteristic curve.

$$P = JV = \left[J_{sc} - J_0 \left(e^{\frac{eV}{KT}} - 1 \right) \right] V$$

The Fill Factor (FF) is a core coefficient for evaluating the quality of the J-V characteristic curve of photovoltaic devices. It directly reflects the efficiency of the device in converting photogenerated carriers into usable electrical energy and is one of the key parameters determining the photoelectric conversion efficiency. The calculation formula is as follows:

$$FF = \frac{P_{max}}{J_{sc} V_{oc}} = \frac{J_{mp} V_{mp}}{J_{sc} V_{oc}}$$

Where the open-circuit voltage (V_{oc}) refers to the voltage across the two terminals of a solar cell under illumination when the output is open-circuited (i.e., with zero current flow). J_{mp} and V_{mp} denote maximum peak current and maximum peak voltage, respectively.

Table S5. The Photovoltaic characteristics(J_{sc}, V_{oc}, J_{mp}, V_{mp}, P_{max}, FF, PCE) of BTO and BTSOS.

Material	J_{sc}(A/m^2)	V_{oc}(V)	J_{mp}(A/m^2)	V_{mp}(V)	P_{max}(W/m^2)	FF	PCE(%)
BTO	103.468	1.855	102.129	1.742	177.938	92.708	14.752
BTSOS	468.843	0.686	450.061	0.603	271.477	84.408	27.138

Note S7: To investigate the coupling mechanism between ion displacement and ferroelectric phase transition in BTSOS, based on modern polarization theory, the variation of macroscopic spontaneous polarization driven by parameter λ during continuous adiabatic phase transition is calculated as follows[12-14]**:**

$$\Delta P = \int_{\lambda_1}^{\lambda_2} \frac{\partial P}{\partial \lambda} d\lambda = P(\lambda_2) - P(\lambda_1)$$

$$P(\lambda) = P_e(\lambda) + P_i(\lambda)$$

$$P_e(\lambda) = -\frac{if|e|}{8\pi^3}\sum_{n=1}^{N}\int_{BZ} dk\left\langle u_{n,k}^{(\lambda)}|\nabla_k|u_{n,k}^{(\lambda)}\right\rangle$$

$$P_i(\lambda) = -\frac{e}{\Omega_0}\sum_{s}^{cell} Z_s^{ion} r_s$$

$$u_{n,k}^{(\lambda)}(r) = e^{iG\cdot R} u_{n,k+G}^{(\lambda)}(r)$$

where P_e represents the electronic polarization, which can be described by the Berry phase of the occupied energy bands. P_i represents ionic polarization, which can be described as the contribution generated by ions with a positive charge of Z_s^{ion} located at atomic positions r_s. N represents the number of occupied energy bands, BZ denotes the Brillouin zone, and f is the occupancy number of occupied states in the valence band. $u_{n,k}^{(\lambda)}$ is the cell-periodic part of the Bloch function, G is an arbitrary vector in the reciprocal lattice, and the sum n runs overall N occupied bands[15].

Table S6: Comparative Analysis of Ps of BTO.

Material	Approaches	P_s(C/m^2)	Ref.
BTO	GGA(PBE-sol)	0.294	This work
	GGA(PBE)	0.39	16
	GGA(PBE-sol)	0.30	16
	HSE	0.37	16
	GGA	0.34	17
	LDA	0.29	18
	LDA	0.273	19
	GGA(PBE-sol)	0.321	20
	GGA(PBE-sol)	0.279	21
	GGA(PBE)	0.47	22
	LDA	0.243	22
	HSE	0.407	22

Table S7. Optimized lattice parameters for BTOS-1b and BTOS-2c.

Material	a(Å)	b(Å)	c(Å)	c/a	α	β	γ	V(Å^3)	Space Group
BTO	3.968	3.968	4.068	1.025	90°	90°	90°	64.050	P4mm
BTOS-1b	4.044	4.044	4.953	1.225	90°	90°	90°	80.986	P4mm
BTOS-2c	4.792	4.792	4.176	0.871	90°	90°	90°	95.904	P4mm

Table S8. Calculated formation energies of BTOS-1b and BTOS-2c.

Material	a(Å)	b(Å)	c(Å)	c/a	α	β	γ	V(Å^3)	Space Group
BTO	3.968	3.968	4.068	1.025	90°	90°	90°	64.050	P4mm
BTOS-1b	4.044	4.044	4.953	1.225	90°	90°	90°	80.986	P4mm
BTOS-2c	4.792	4.792	4.176	0.871	90°	90°	90°	95.904	P4mm

Figure S1. BTO models with S substituting for O at the 1b and 2c sites, respectively. (a) BTOS-1b, (b) BTOS-2c.

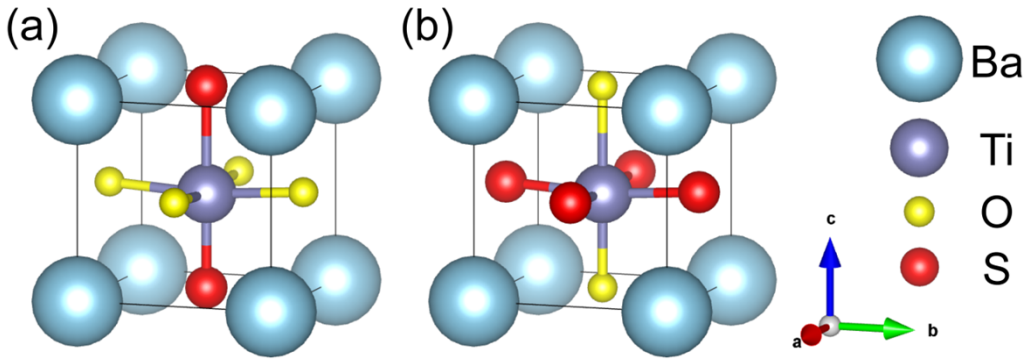

Figure S2. A 2×2×2 BTO model constructed with a Sn substituting for a Ti and a S substituting for O at both the 1b and 2c sites, respectively. (a) BTSOS-1b, (b) BTSOS-2c.

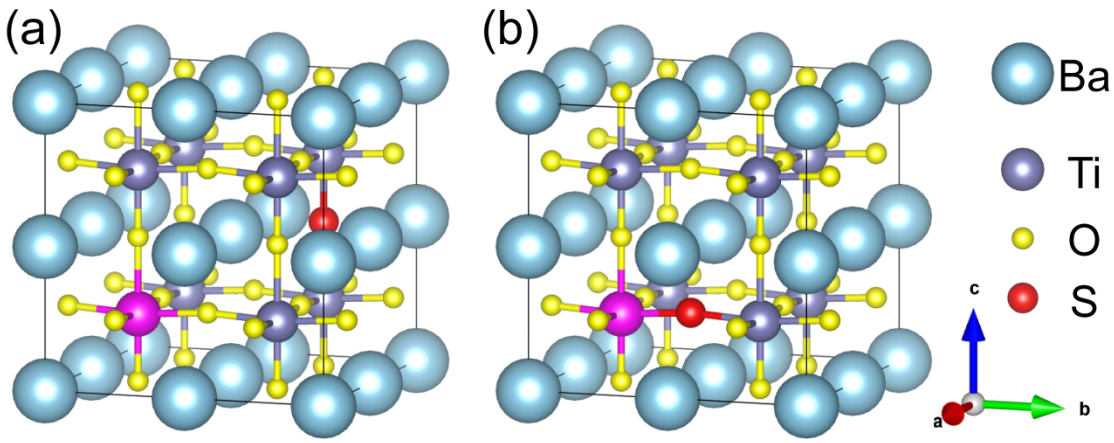

Figure S3. Energy variation curve of BTSOS simulated using the AIMD method at 300 K.

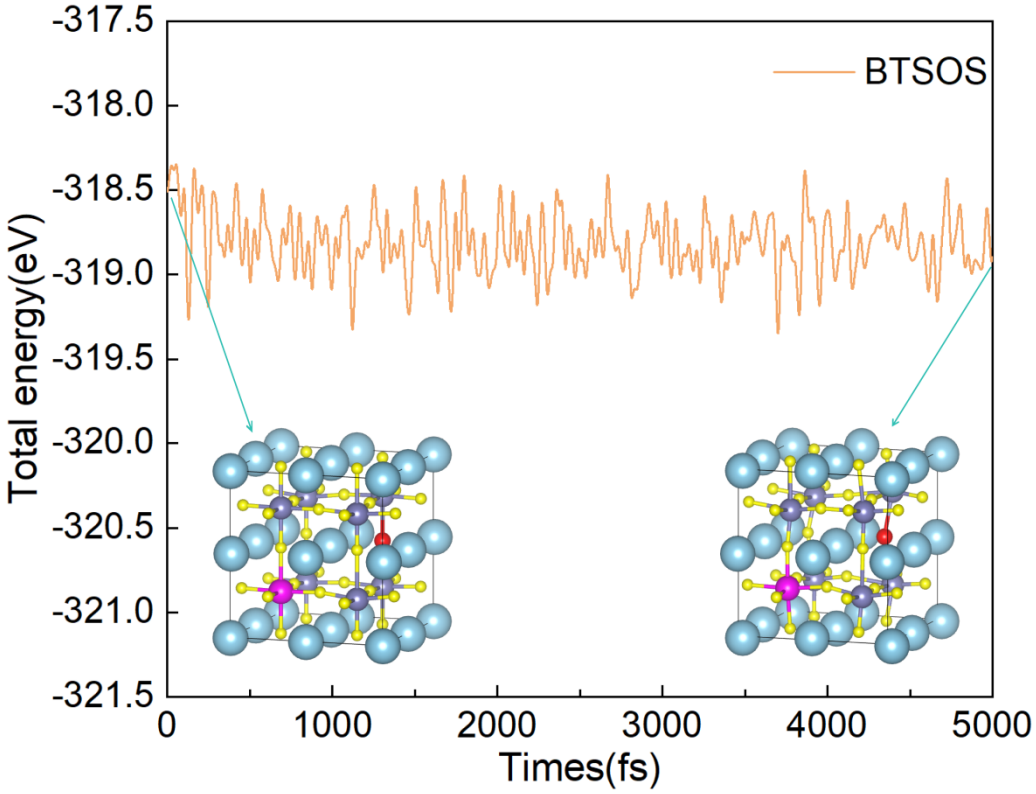

Figure S4: Temperature-dependent variations of the ferroelectric double-well potential: (a) BTO; (b) BTSOS.

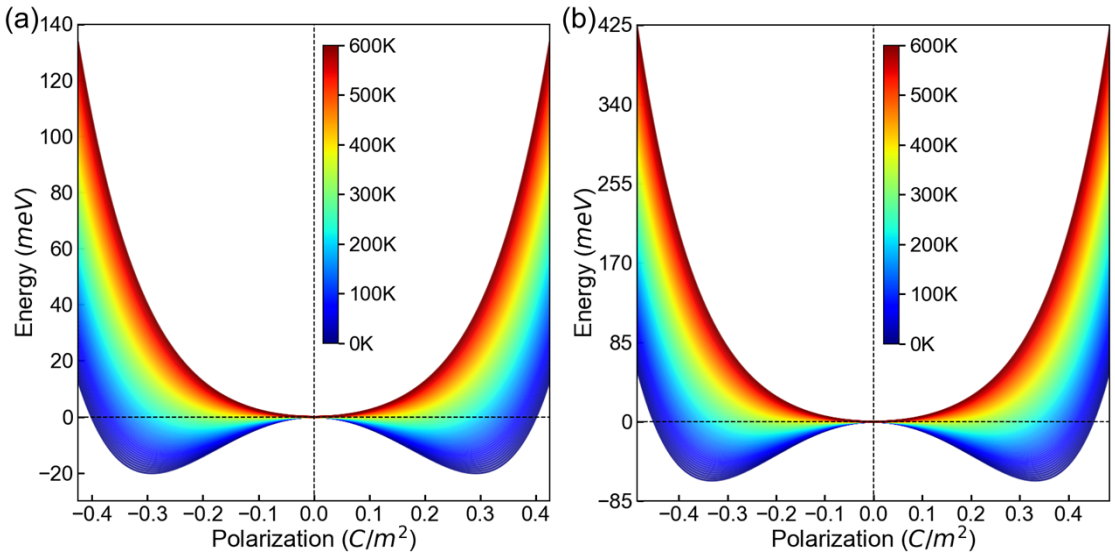

References

1. J. Long, L. Yang and X. Wei, *J. Alloy. Compd.*, 2013, **549**, 336-340.
2. G. J. Fischer, Z. Wang and S.-i. Karato, *Physics and Chemistry of Minerals*, 1993, **20**, 97-103.
3. M. Gajdoš, K. Hummer, G. Kresse, J. Furthmüller and F. Bechstedt, *Physical Review B*, 2006, **73**, 045112.
4. P. Johari and V. B. Shenoy, *ACS Nano*, 2011, **5**, 7640-7647.
5. M. J. Patel, S. K. Gupta and P. N. Gajjar, *J. Phys. Chem. Solids*, 2023, **176**, 8.
6. Y. H. Zhao, J. H. Jing, L. W. Chen, F. H. Xu and H. Hou, *Acta Metall. Sin.*, 2021, **57**, 1107-1125.
7. X. L. Zhang, Y. B. Tang, F. Zhang and C. S. Lee, *Adv. Energy Mater.*, 2016, **6**, 6.
8. M. Radak, *Reference Air Mass 1.5 Spectra*, 2022.
9. Green and M. A, *Solar Energy*, 1982, **-1**.
10. M. Wang, C. Jiang, S. Zhang, X. Song, Y. Tang and H.-M. Cheng, *Nature Chemistry*, 2018, **10**, 667-672.
11. X. Xu, Y. Dong, Q. Hu, N. Si and C. Zhang, *Energy & Fuels*, 2024, **38**, 7579-7613.
12. R. D. King-Smith and D. Vanderbilt, *Physical Review B*, 1993, **47**, 1651-1654.
13. R. Resta and D. Vanderbilt, in *Physics of Ferroelectrics: A Modern Perspective*, Springer Berlin Heidelberg, Berlin, Heidelberg, 2007, DOI: 10.1007/978-3-540-34591-6_2, pp. 31-68.
14. S. F. Yuk, K. C. Pitike, S. M. Nakhmanson, M. Eisenbach, Y. W. Li and V. R. Cooper, *Sci Rep*, 2017, **7**, 43482.
15. R. Resta, *Ferroelectrics*, 1992, **136**, 51-55.
16. F. Jia, S. Xu, S. Hu, J. Chen, Y. Wang, Y. Li, W. Ren and J. Cheng, *npj Computational Materials*, 2025, **11**, 6.
17. Z. Miao, L. Chen, R. Wang, R. Yuan, F. Zhou, P. Lv, X. Zhang and Q. Wang, *Materials Research Express*, 2018, **5**, 025505.
18. J. J. Wang, F. Y. Meng, X. Q. Ma, M. X. Xu and L. Q. Chen, *Journal of Applied Physics*, 2010, **108**, 034107.
19. M. Mirseraji and M. G. Shahraki, *Physica B: Condensed Matter*, 2018, **538**, 120-130.
20. S. Amounas, A. Hbab, H. Chaib and T. Ait-Taleb, *Physica B: Condensed Matter*, 2023, **663**, 415002.
21. A. Ali, I. Khan, Z. Ali, F. Khan and I. Ahmad, *International Journal of Modern Physics B*, 2019, **33**, 1950231.
22. Y. Zhang, J. Sun, J. P. Perdew and X. Wu, *Physical Review B*, 2017, **96**, 035143.